THE 10 FEBRUARY 1977 LUNAR OCCULTATION OF URANUS. RADIUS, LIMB DARKENING, AND POLAR BRIGHTENING AT 6900 Å.

R. R. RADICK AND W. C. TETLEY

(NASA-CR-158780) THE 10 FEBRUARY 1977 LUNAR OCCULTATION OF URANUS. RADIUS, LIMB DARKENING, AND POLAR BRIGHTENING AT 6900 A (Illinois Univ.) 23 p HC A02/MF A01 CSCL 03A G3/89
N79-28074
Unclas
29261

THE 10 FEBRUARY 1977 LUNAR OCCULTATION OF URANUS. RADIUS, LIMB DARKENING, AND POLAR BRIGHTENING AT 6900 Å.

Richard R. Radick and William C. Tetley

Astronomy Department
University of Illinois
Urbana, Illinois 61801

Manuscript pages: 16

Figures: 4

Tables: 2

RUNNING HEAD: LUNAR OCCULTATION OF URANUS

DIRECT CORRESPONDENCE TO:

Richard R. Radick
Astronomy Department
University of Illinois
Urbana, Illinois 61801

ABSTRACT

A photoelectric observation in the near infrared of the 10 February 1977 lunar occultation of Uranus is described and analyzed in terms of planetary radius, limb darkening, and polar brightening. Contact timings, corrected for lunar limb effects, indicate an equatorial radius of 25700 ± 500 km for the visible disk. A modified Minnaert function is used to model limb darkening and polar brightening. Least-squares fits to the observed light curve indicate that Uranus is slightly limb darkened in the passband of the observations (450 Å FWHM centered near 6900 Å) and that polar brightening is present.

I. INTRODUCTION

Although Uranus has been regularly observed for almost two centuries, many of its physical characteristics remain poorly known. Normally, ground-based telescopes cannot clearly resolve the planet because atmospheric seeing distorts and blurs its small image.

The photographs obtained by Danielson et al. (1972), using the balloon-borne Stratoscope II telescope, have provided the best modern information about the appearance of Uranus in the visual region of the spectrum. These photographs show a strongly limb darkened disk, which is otherwide featureless, having an equatorial radius of 25900 ± 300 km. Recent re-analysis of the Stratoscope II images by Avis et al. (1978) shows the ellipticity of the disk to be 0.021 ± 0.001. The 1977 occultation of SAO 158687 by Uranus yielded at measurement of 26200 ± 100 km for the radius at the half-light level (Elliot et al., 1978). However, the half-light radius is not the radius of the visible disk, but something several hundred kilometers larger. Accordingly, this result is consistent with the Stratoscope II measurement.

The appearance of the Uranian disk is considerably different in the infrared. Sinton (1972) and Smith (1977), observing in the 8370 Å methane band, and Franz and Price (1977; also Price and Franz, 1978), observing in the 7300 Å band, have found the disk to be limb brightened at these wavelengths. These observers also find brightness variations across the disk, both in the methane bands and in the adjacent continua, which are best explained as a general brightening over the polar region of the planet.

On several occasions during 1976 and 1977 Uranus was occulted by the moon. One of these events, the reappearance of 10 February 1977, was visible from North America under favorable circumstances. Since the spatial resolution afforded by an occultation is virtually unaffected by atmospheric

seeing, this valuable opportunity was used to learn more about the appearance of the Uranian disk in the near infrared.

II. OBSERVATION

The February 10 occultation was observed at the University of Illinois Prairie Observatory using the high-speed digital recording system which has been described elsewhere (Radick, 1979). The bandpass of the observation is shown as Figure 1. The shape is due primarily to the spectral filter which was used. Although the region spanned by this response includes the wings of two strong methane bands at 6700 Å and 7300 Å and a pair of weaker bands, it is principally the continua lying between these absorption features which are represented by the observation.

At the time of the occultation, the third quarter moon was 31 degrees above the horizon at Prairie Observatory. The sky transparency was good, although the seeing was rather disturbed (∿4") and scintillation was quite pronounced. Telescope pointing was achieved by tracking a nearby star until shortly before the time predicted for emersion and then off-setting to the position of the planet. In order to minimize the chances for an unfortunate outcome, the event was viewed through a comparatively large (24") diaphragm. This insurance was dearly paid for in terms of scattered moonlight entering the photometer, Uranus contributing only about 12% of the total light. In fact, visual inspection after emersion showed the planet to be well-centered in the diaphragm.

The observational trace is shown as Figure 2. Each point represents the sum of sixty-four 1 msec time frames. Two low-order bits were truncated from each time frame during the observation: the ordinate scale does not correct for this truncation. The abscissa is scaled in relative time units, the origin corresponding to 9:32:00.0 UTC with an uncertainty of perhaps

¼ second (Radick, 1979). Relative time intervals are precise. The sloping baseline is due to a gradual decrease in background light as the bright portion of the moon moved away from the photometer aperture. Scintillation, in the form of increasing noise, becomes apparent as the planet emerges.

III. ANALYSIS AND RESULTS

A. Correction and Normalization of the Observational Data.

The observational data were first corrected for coincidence losses due to a system bandwidth of 20 MHz. A linear baseline was then fitted by least squares to those points which clearly lay outside the occultation event and removed from the observational trace. The ordinate was then rescaled to unit amplitude. The central portion of the corrected trace is shown as Figure 3. The corrected trace shows no features which indicate that removal of a higher-order baseline is required. This impression is consistent with the experience of Elliot et al. (1975) in their analyses of lunar occultations involving the satellites of Saturn.

It is unnecessary to correct the trace for any effects due to the truncation of the observational data. This truncation is responsible for a small portion of the noise in the normalized light curve, but it does not distort its shape.

B. Lunar Limb Corrections.

The topography of the lunar limb can significantly influence the detailed shape of the light curve for planetary occultations. If the lunar velocity vector in the plane of the sky is not approximately perpendicular to the limb at the point of contact, the occultation can "slide" several kilometers along the lunar limb. The Uranus

occultation involved about 12 km of limb. On this scale, curvature of the mean limb also becomes significant. Together, local features on the limb and limb curvature may produce appreciable variations in the angular rate at which an occultation proceeds. Since it is the angular rather than the temporal scale of the event which is of ultimate interest, the relationship between the two must be carefully examined.

For a stellar occultation, it is normally possible to determine the angular velocity of the lunar limb at the point of contact directly from the diffraction fringe pattern. This approach cannot be used in the present case, however. Due to the large angular size of the planet, there simply are no detectable diffraction effects in these data. Therefore, we are forced to rely on predictions for the information necessary to convert the temporal scale of the observation into angular measure.

Accordingly, we have calculated topocentric positions and distances for the moon and Uranus, librations, and the position angle of the lunar axis for each second over an interval of about thirty seconds centered on the midpoint of the occultation by interpolating the geocentric data tabulated in The American Ephemeris and Nautical Almanac and applying the appropriate parallactic corrections. From these, topocentric values for the direction and angular rate of the apparent lunar motion, as well as values for the angular separation and position angle of Uranus measured relative to the center of the moon, were derived as functions of time. The results of these calculations are compared with the U. S. Naval Observatory's prediction for the midpoint of the occultation in Table I. The differences present among the entries in Table I may reflect any of a variety of things: ephemeris differences, interpolation round-off errors, truncation errors in computation, or differences in the precepts used for the calculations.

It is probably reasonable to suppose that these differences are representative of the uncertainties in the circumstances of the occultation, namely ±1 sec in time and ±0.1 degree in angle. The fact that the midpoint of the occultation occurred within one second of the predicted time lends assurance to these calculations.

The geometry of the occultation may be conveniently referred to a Cartesian co-ordinate system fixed to the lunar limb, as shown in Figure 4. The origin of this system has been arbitrarily placed at Watts' Angle 219.0, near the location of the central emersion. The ordinate axis intersects the center of the moon. Both axes are scaled in arcseconds. Both limb curvature and elevation changes relative to the mean limb as read from the Watts' charts (Watts, 1963; Van Flandern, 1970) contribute to the limb contour shown. The trajectories labeled A and B are drawn in the direction of the apparent lunar motion relative to this co-ordinate system. Trajectory A represents the circumstances we predict. Trajectory B corresponds approximately to the USNO prediction. One may consider either the lunar limb moving down and away from Uranus, or Uranus rising above the limb, along the direction of these lines.

If it is assumed that the central emersion occurred at the predicted time, then the location of Uranus along these trajectories and the angular distance between the center of the planet and the lunar limb contour can be specified at any instant of time from the results of the calculations described above. In other words, the temporal scale of the observation can be converted to the desired angular scale. Unfortunately, neither the circumstances of the occultation nor the details of the limb profile are known to sufficient accuracy to allow the calculation of an exact conversion. Accordingly, we shall perform the remaining analysis for each of the two

trajectories. In addition, we will consider models which assume a smoothly curved lunar limb, in order to assess the influence of the Watts' corrections on our results.

C. Model Occultation Curves.

The shape of the corrected trace provides information about the brightness distribution over the disk of the planet. We expect this distribution to reflect limb brightening/darkening and, perhaps, polar brightening. We assume that the limb brightening/darkening obeys the Minnaert Law (Binder and Jones, 1972; Binder and McCarthy, 1973; Elliot et al., 1975), which states that the intensity observed from any point on the disk is proportional to

$$\cos^{k}(i) \cdot \cos^{k-1}(e)$$

where i is the irradiation angle and e the emission angle for that point. The parameter k characterizes the nature of the limb brightening/darkening: assuming i = e, the disk appears limb darkened if $k > 0.5$, uniformly illuminated if $k = 0$, and limb brightened if $k < 0.5$. To represent polar brightening, we multiply the Minnaert Law by a function $B(\phi)$, where ϕ is Uranian latitutde. Currently, there is virtually no information available indicating what the functional form of $B(\phi)$ may be. Accordingly, we shall consider three rather arbitrary possibilities. The first.

$$B(\phi) = 1, \text{ (Model 1)}$$

implies no polar brightening. The second,

$$B(\phi) = 1 + B(1 - \cos \phi), \text{ (Model 2)}$$

was chosen because it suggests a "bright polar cap". The third,

$$B(\phi) = 1 + B \sin(|\phi|), \quad \text{(Model 3)}$$

suggests a "dark equatorial belt". The parameter B measures the increase in brightness at the pole relative to that at the equator for zero phase angle.

We have constructed numerical models for the occultation light curve which envision a hypothetical occulting straight edge being drawn across the planet, revealing its disk in evenly-spaced steps. We subdivide the disk of the planet into square cells. A particular cell is considered part of the disk if its center lies inside the boundary of the disk. Tests demonstrated that subdivisions of fifteen and twenty-five cells/disk diameter yield essentially identical results; consequently, the coarser subdivision has been used throughout these calculations. The angles i, e, and ϕ were evaluated for the midpoint of each cell within the disk and model brightness distributions calculated over a range of values for k and B. Normalized occultation curves were then constructed from these distributions by summing brightness contributions from rows of cells parallel to the occulting edge, summing the resulting strip brightnesses, and finally normalizing to the fully illuminated disk. This procedure produces models evaluated at sixteen evenly-spaced points, the two endpoints having zero and unit intensities. Continuous curves were constructed from these discrete models using cubic spline functions. These continuous models were then compared to the corrected observational trace. Best-fit values for the contact points were identified which minimized the χ^2/(degree-of-freedom) for each continuous model. The overall best fit was then selected, using the same criterion, by means of a grid search in k and B. The intervals of this search were

0.05 units for k and 0.2 or 0.4 units for B. In this fashion, we ultimately identify best-fit models characterized by four fitted parameters, namely, the two contact points, the Minnaert parameter, and the polar brightening parameter.

In view of the uncertainties in the lunar limb corrections and the effects these alone have on our results (which will become evident presently), it is unnecessary to correct for either the ellipticity or the illumination defect of the Uranian disk. The projected ellipticity is about 0.007, and the chord defined by the contacts is less than 0.5% shorter than the equatorial diameter for the fully illuminated disk. The illumination defect produced by the 3^{o} phase angle between the sun and the Earth, as seen from Uranus, shortens this chord by another 0.1%. Such effects do not appreciably influence our analysis.

D. Results

In all eighteen best-fit models were calculated as follows:

1) For each of the two trajectories shown in Figure 4, best fits were calculated for the three polar brightening models described above. 2) These calculations were repeated, holding the contact interval fixed at a value corresponding to a radius of 25900 km for the visible disk (i.e., the Stratoscope II radius). 3) A third set of six models was computed assuming the circumstances of Trajectory A and a smoothly-curved lunar limb (i.e., no Watts' corrections were applied). The results of these calculations are summarized in Table II. The uncertainties tabulated therein were determined from the curvature of the χ^2 surface at its minimum with respect to the parameters and may be regarded as formal standard errors (Orear, 1958). The values for the radius have been determined from the contact intervals, assuming a topocentric distance of 18.367 A.U. to Uranus.

These results are illustrated in Figure 3, which shows the best-fit curves for polar brightening Models 1 and 2 of Trajectory A superimposed on the normalized observational light curve. Model 3 is virtually indistinguishable from Model 2, and is not shown. The results are similar for Trajectory B and also for Trajectory A without the Watts' corrections; that is, all the best fits for Model 1 resemble one another, as do the fits for all models which incorporate polar brightening.

IV. CONCLUSIONS AND DISCUSSION

We draw the following conclusions from the results presented in Table II:

(1). The data are well-fitted. However, a significant improvement in the fit is achieved when polar brightening is incorporated into the model, as judged from the magnitudes of the χ^2/(degree-of-freedom) for the various best-fits.

(2). The fit does not distinguish between polar brightening Models 2 and 3. We suspect that these data cannot provide much detailed information about the polar brightening on Uranus, and that any reasonable model for polar brightening would probably reproduce the observational light curve as well as do these two.

(3). The results of the analysis are not significantly affected by the uncertainties in either the circumstances of the occultation or the detailed shape of the lunar limb profile as read from the Watts' charts. This is least true for the polar brightening parameter, which suffers changes as large as 40% from these effects. The values derived for the planetary radius and the Minnaert parameter are comparatively stable.

(4). The amount of polar brightening demanded by the best-fit models seems

uncomfortably large, even though Price and Franz report "significant" amounts of polar brightening in and near the 7300 Å methane band. To check this impression, the brightness distributions specified by our models were numerically smeared to simulate aperture and seeing effects. Model "pinhole scans" were then calculated from these smeared distributions and compared visually to the area-scanning photometric observations obtained at Lowell Observatory (Franz and Price, 1977; Price and Franz, 1978). These experiments suggest that the area-scanning observations might be consistent with values for B one-third to one-half those demanded by our best-fit models, but not much more. Although we do not dismiss the possibility that the larger values obtained here are correct, it seems prudent to acknowledge that our analysis may overestimate the magnitude of the polar brightening. Whether this would reflect uncertain limb corrections, or some systematic effect which has been overlooked entirely, or the selection of an inappropriate functional form for the polar brightening, is difficult to decide.

(5). Averaging the results for Trajectories A and B, Models 2 and 3, we obtain 25550 ± 500 km for the radius of the Uranian disk, assuming circular symmetry. Correction for ellipticity and illumination defect yields a value of about 25700 km for the equatorial radius. While not particularly accurate, this result is consistent with the Stratoscope II measurement. On the other hand, the radius inferred from Model 1 (no polar brightening) does not appear to be consistent with the Stratoscope II radius. This discrepancy strengthens the case for polar brightening.

(6). In the same manner, we obtain an averaged value of 0.50 ± 0.07 for the Minnaert parameter. In view of the possibility that we have overestimated the numerical magnitude of the polar brightening, we have examined in

detail what happens to the best-fit models as B is decreased. The initial adjustment appears to be at the expense of the planetary radius, which becomes progressively smaller as B is decreased. Only as B approaches zero does the value of the Minnaert parameter begin to respond by increasing in value. We estimate that a factor-of-two decrease in B from the best-fit values increases k by about 0.05 units. A similar increase occurs if we assume the Stratoscope II radius. Making these allowances, we feel that a value of 0.60 ± 0.10 is appropriate for the Minnaert parameter, which in turn implies that Uranus is slightly limb darkened in the passband of our observation. This conclusion is consistent with the results of Price and Franz.

In summary, we have presented high-resolution observational evidence, free from the distorting effects of atmospheric seeing, which confirms the presence of visible structure on the disk of Uranus. This structure can be represented by a one-parameter polar brightening model plus limb darkening, although some difficulties remain in assigning a quantitative magnitude to the polar brightening. The analysis results in an accurate quantitative measure of the limb darkening displayed by the disk in the passband of our observation.

ACKNOWLEDGEMENTS

The occultation predictions prepared and distributed by the U. S. Naval Observatory were of great value both in the observation and the analysis of this event. We particularly wish to acknowledge this assistance. John Dickel provided continuing encouragement and critical advice during the course of the analysis. This work was supported in part by the National Aeronautics and Space Administration under Grant NGR14-005-176. Funds for computation were provided by the University of Illinois Research Board.

REFERENCES

Avis, C., Lorre, J., Lynn, D., Colombo, G., and Franklin, F. (1978). A New Analysis of the Stratoscope II Images of Uranus. Bull. Amer. Astron. Soc. 10, 576.

Binder, A. B., and Jones, J. C. (1972). Spectrophotometric Studies of the Photometric Function, Composition, and Distribution of the Surface Materials of Mars. J. Geophys. Res. 77, 3005-3020.

Binder, A. B., and McCarthy, D. W. (1973). IR Spectrophotometry of Jupiter and Saturn. Astron. J. 78, 939-950.

Danielson, R. E., Tomaski, M. G., and Savage, B. D. (1972). High-resolution Imagery of Uranus Obtained by Stratoscope II. Astrophys. J. 178, 887-900.

Elliot, J. L., Dunham, E., Wasserman, L. H., Millis, R. L., and Churms, J. (1978). The Radii of Uranian Rings α, β, γ, δ, ε, η, 4, 5, and 6 from their Occultation of SAO 158687. Astron. J. 83, 980-992.

Elliot, J. L., Veverka, J., and Goguen, J. (1975). Lunar Occultation of Saturn I. The Diameters of Tethys, Dione, Rhea, Titan, and Iapetus. Icarus 26, 387-407.

Franz, O. G., and Price, M. J. (1977). Uranus: Limb and Polar Brightening at 7300 Å. Astrophys. J. 214, L145-146.

Orear, J. (1958). Notes on Statistics for Physicists. Univ. of California Radiation Lab., Berkeley.

Price, M. J., and Franz, O. G. (1978). Limb Brightening on Uranus: The Visible Spectrum, II. Icarus 34, 355-373.

Radick, R. R. (1979). The 20 October 1977 Lunar Occultation of Beta Capricorni. Astron. J. 84, 257-258.

References (continued)

Sinton, W. M. (1972). Limb and Polar Brightening of Uranus at 8870 Å. Astrophys. J. 176, L131-133.

Smith, B. A. (1977). Uranus Photography in the 890-nm Absorption Band of Methane. Bull. Amer. Astron. Soc. 9, 744-745.

Van Flandern, T. C. (1970). Some Notes on the Use of the Watts Limb-Correction Charts. Astron. J. 75, 744-746.

Watts, C. B. (1963). The Marginal Zone of the Moon. Astron. Papers Am. Ephem. 17.

Table I

Predicted Circumstances for Midpoint of Uranus Occultation

Circumstance	USNO Predictions	Present Calculation
Time (UTC, 10Feb77)	9:32:49	9:32:50
Position Angle (PA)	238.2	238.1
Contact Angle (CA)	-126.8	-126.8
Watts' Angle (WA)	219.1	219.0
Long. Lib.	-0.3	-0.4
Lat. Lib.	-1.0	-1.0
Shadow Velocity	0.4520 km/sec	0.4524 km/sec

TABLE II

Trajectory	Polar Brightening Model	Radius(km)	Minnaert Parameter	Polar Brightening Parameter	χ^2/(Degree of Freedom)
A	1	25000 ± 200	0.65 ± 0.05	None	0.976
A	2	25400 ± 200	0.55 ± 0.05	1.2 ± 0.1	0.920
A	3	25400 ± 200	0.45 ± 0.04	2.0 ± 0.2	0.922
A	1	25900 (Fixed)	0.80 ± 0.05	None	0.989
A	2	25900 (Fixed)	0.60 ± 0.04	1.4 ± 0.1	0.922
A	3	25900 (Fixed)	0.50 ± 0.04	2.0 ± 0.2	0.924
B	1	24000 ± 200	0.55 ± 0.04	None	0.992
B	2	26300 ± 200	0.55 ± 0.04	1.6 ± 0.1	0.920
B	3	25100 ± 200	0.40 ± 0.04	2.8 ± 0.3	0.923
B	1	25900 (Fixed)	0.85 ± 0.05	None	0.999
B	2	25900 (Fixed)	0.60 ± 0.04	1.6 ± 0.1	0.922
B	3	25900 (Fixed)	0.50 ± 0.04	3.4 ± 0.4	0.926
A+	1	26000 ± 200	0.60 ± 0.04	None	0.990
A+	2	26800 ± 200	0.50 ± 0.04	1.4 ± 0.1	0.919
A+	3	26800 ± 200	0.40 ± 0.04	2.4 ± 0.2	0.923
A+	1	25900 (Fixed)	0.55 ± 0.04	None	0.992
A+	2	25900 (Fixed)	0.40 ± 0.04	1.4 ± 0.1	0.924
A+	3	25900 (Fixed)	0.35 ± 0.04	2.0 ± 0.2	0.927

+No Watts' corrections.

FIGURE CAPTIONS

FIG. 1. - The bandpass of the observation.

FIG. 2. - The uncorrected observational light curve.

FIG. 3. - The normalized observational light curve, and two representative best-fit model light curves.

FIG. 4. - The geometry of the occultation. The curving arc near the abscissa represents the lunar limb, which is moving away (down) from the center of the planet at this time. The cardinal directions in the sky and the location of the north Uranian pole are indicated.

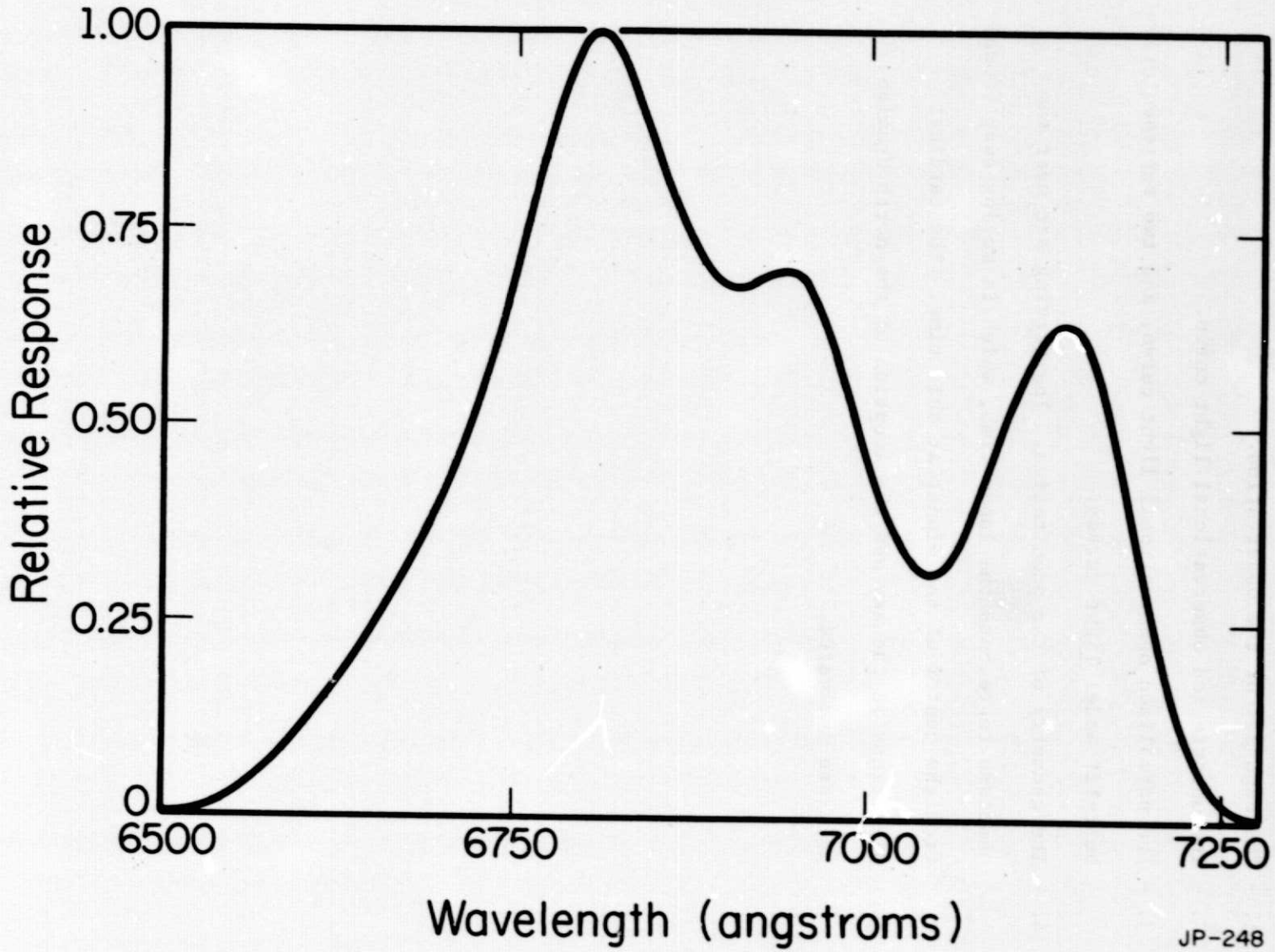
1.00
0.75
0.50
0.25
0
Relative Response
6500
6750
7000
7250
Wavelength (angstroms)
JP-248

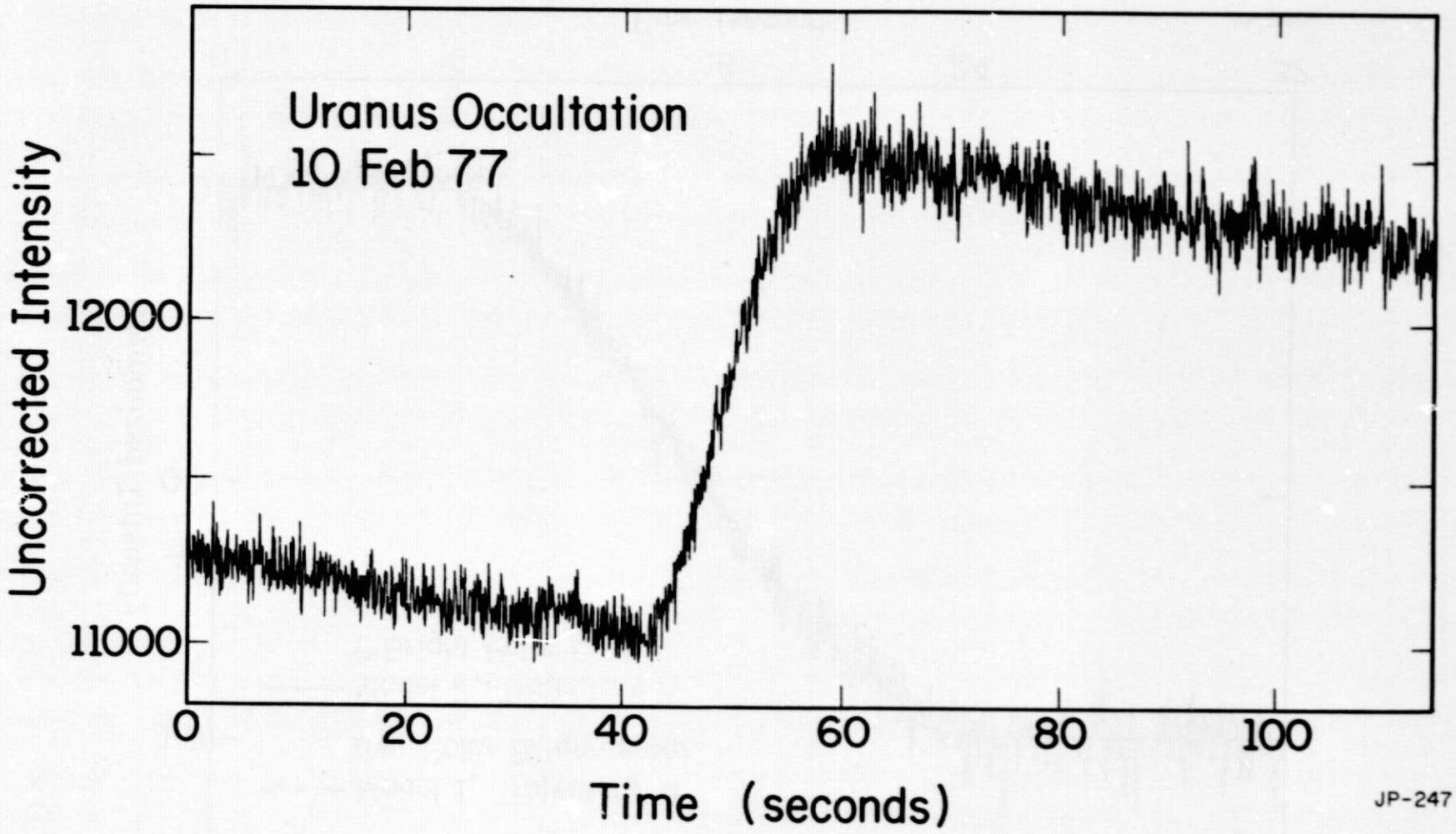
Uranus Occultation
10 Feb 77
Uncorrected Intensity
12000
11000
0
20
40
60
80
100
Time (seconds)
JP-247

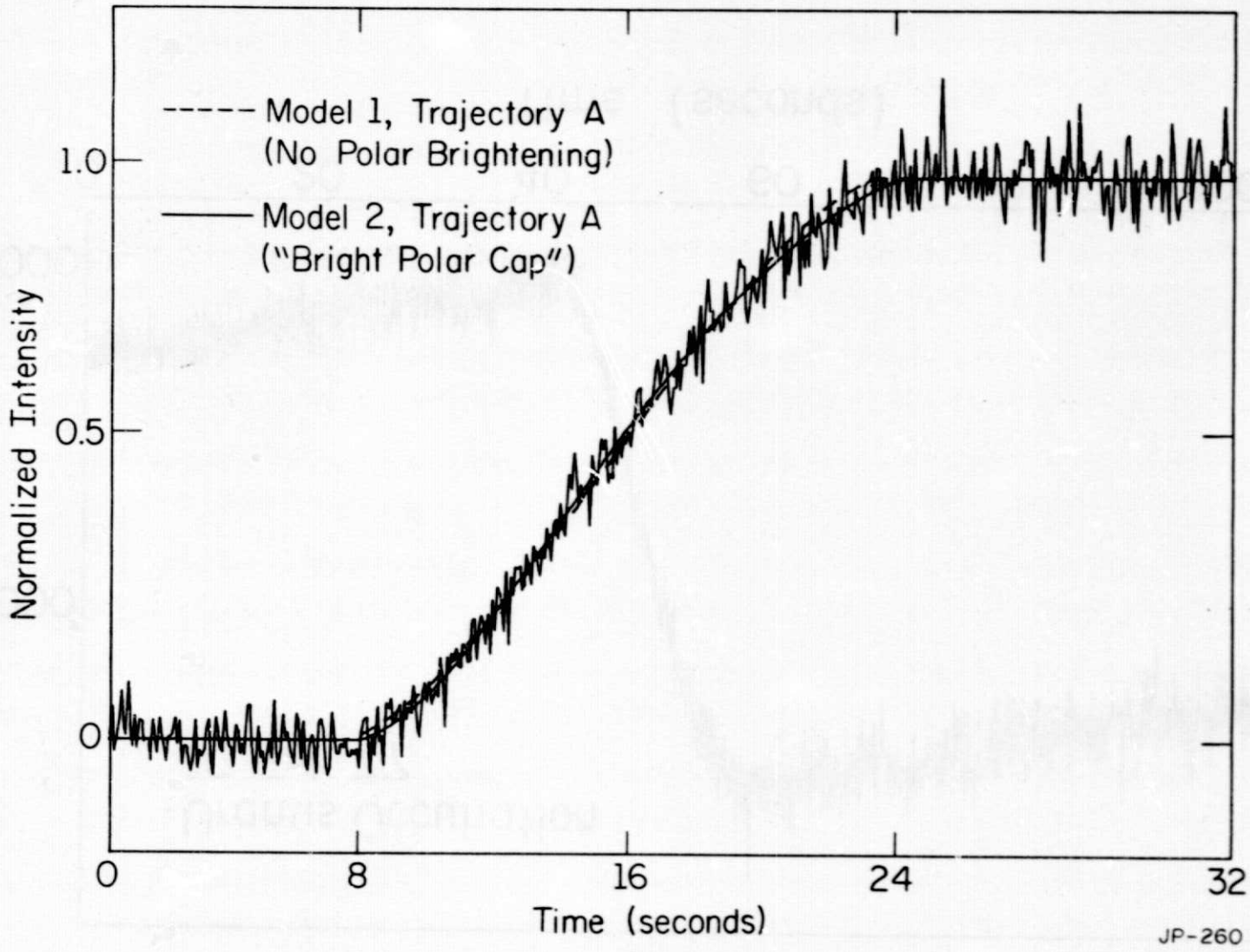
----- Model 1, Trajectory A
(No Polar Brightening)
—— Model 2, Trajectory A
("Bright Polar Cap")
Normalized Intensity
1.0
0.5
0
0
8
16
24
32
Time (seconds)
JP-260

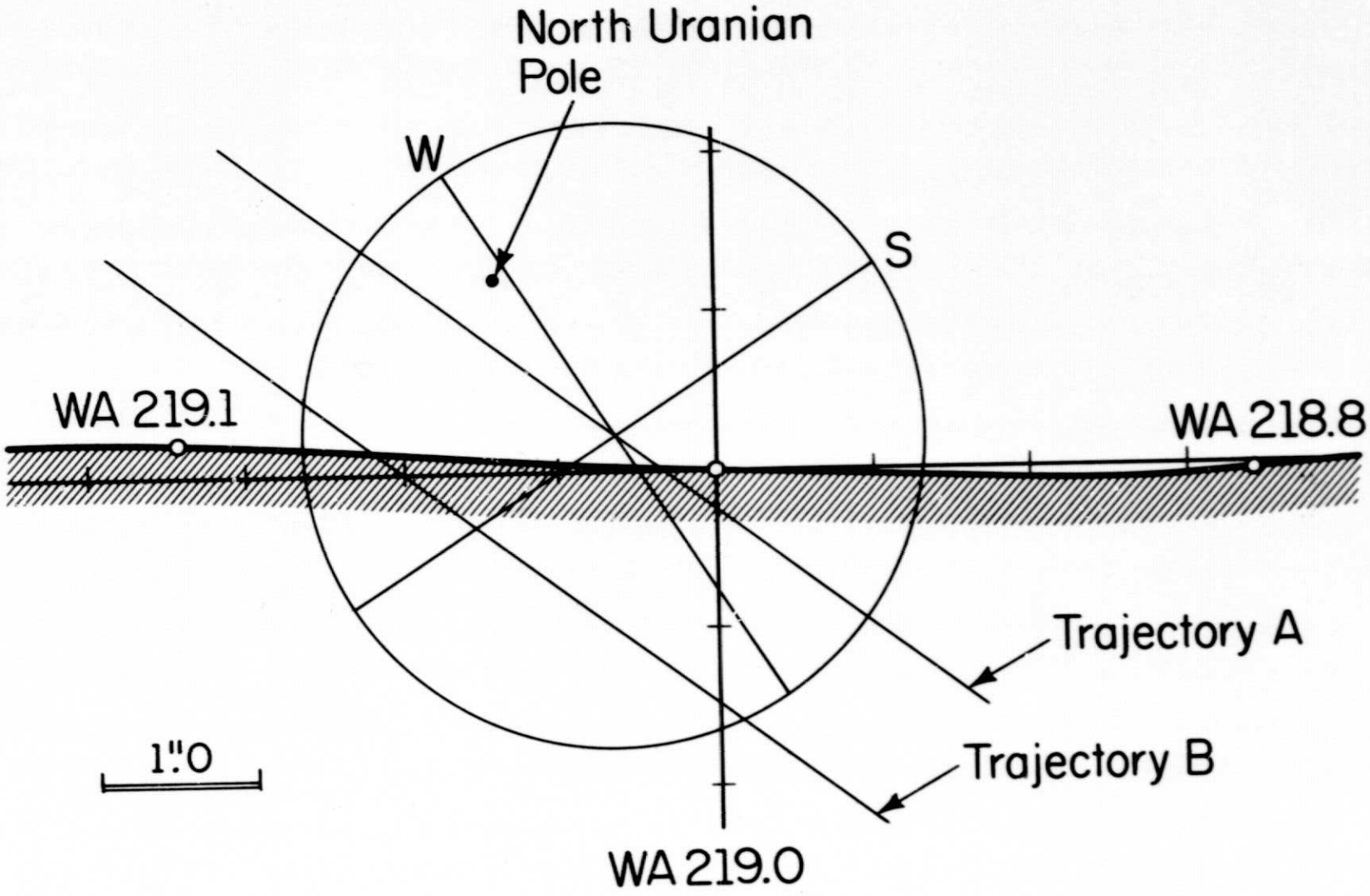
North Uranian
Pole
W
S
WA 219.1
WA 218.8
Trajectory A
Trajectory B
1"0
WA 219.0
JP-249